Inversion of angle-resolved photoemission measurements in high-T_c cuprates

S. Verga, A. Knigavko, and F. Marsiglio

Department of Physics, University of Alberta, Edmonton, Alberta, Canada T6G 2J1

Recent energy dispersion measurements in several families of the hole-doped copper oxides have revealed a kink in the energy vs momentum relation. These have tentatively been identified as due to electron-phonon coupling. We invert this data directly to determine the bosonic spectral function; the kink gives rise to a singular function in the phonon energy region.

The determination of mechanism for superconductivity in the high-temperature oxides has occupied researchers for the past 15 years. The most definitive signatures for determining the mechanism in conventional superconductors traditionally have been the measurement of the single-particle tunneling *I-V* characteristic[1] and the concomitant inversion procedure.[2] Researchers[3] have reported some success with this procedure for the high-temperature superconductors; nonetheless the applicability of such a procedure is unknown outside a weak-coupling electron-phonon framework, and the process is complicated in the superconducting state due to the nonisotropic nature of the order parameter. Other procedures have been suggested, such as the inversion of the normal-state optical conductivity,[4] the conductivity in the superconducting state in conjunction with neutron-scattering data,[5] and the inversion of photoemission data[6] in the superconducting state. The recent very high-resolution photoemission measurements on a variety of cuprate materials have suggested that a sizable electron-phonon coupling exists,[7] and the possibility of inverting this data (in the normal state) has been reopened. In this paper, we outline an inversion procedure, determine the "bosonic spectrum" to which the electrons are coupled, and assess the possibility that these bosons are the phonons. The data for the dispersion for three different dopant concentrations in La$_{2-\delta}$Sr$_\delta$CuO$_4$ (LSCO) is reproduced in Fig. 1.[7] Particularly for the underdoped sample there is a well-defined kink that occurs at approximately 70 meV. Lanzara *et al.*[7] attributed this kink to an electron self-energy effect due to coupling to phonons. We wish to investigate this claim based on some microscopic models.

We first examine the result obtained from "standard" phonon models, namely, the Einstein and Debye models. Each in turn is used to model the electron-phonon spectral function $\alpha^2F(\nu)$, and then, within the standard framework,[8,9] the electron self-energy $\Sigma(\omega) \equiv \Sigma_1(\omega) + i\Sigma_2(\omega)$ is obtained (at $T=0$):

$$\Sigma_1(\omega + i\delta) = \int_0^\infty \alpha^2 F(\nu) \ln\left|\frac{\omega - \nu}{\omega + \nu}\right| d\nu \qquad (1)$$

from which the electron dispersion E_k can be obtained,

$$E_k = \epsilon_k + \Sigma_1(E_k), \qquad (2)$$

where ϵ_k is the bare (with respect to electron-phonon interactions) quasiparticle energy. The model spectrum, along with the real part of the self-energy and the dispersion is

plotted in Figs. 2 and 3 for the Einstein and Debye models, respectively. Note that for some values of ϵ_k the dispersion as shown is multivalued. This is because multiple poles exist in these regions. In fact, the spectral function generally evolves in the following manner[8] (we use the Einstein model depicted in Fig. 2 for simplicity): at low energies a pole exists just above the real axis (i.e., with infinitesmal width). What is not depicted in Figs. 2 or 3 is that the weight of this pole (i.e., the residue) goes to zero as $|\epsilon_k| \to \infty$. So, beyond about $|\epsilon_k| \approx 140$ meV, the weight of this pole becomes very small. The actual energy (E_k) at this point becomes very nearly the Einstein frequency. In a sense the electrons and phonons have "hybridized" and this branch, which started out very "electron like" near $E_k \approx 0$, is now very "phonon-like." The branch just below -80 meV in Fig. 2(c) is more or less irrelevant, since the self-energy has a very large imaginary part [see Fig. 2(b)]. Finally, as $|\epsilon_k|$ continues to increase the lowest branch begins to dominate. In this limit this branch becomes very "electronlike" albeit with a finite width.

In addition, in the case of the Einstein spectrum there is an unphysical singularity. While this is easily washed out by
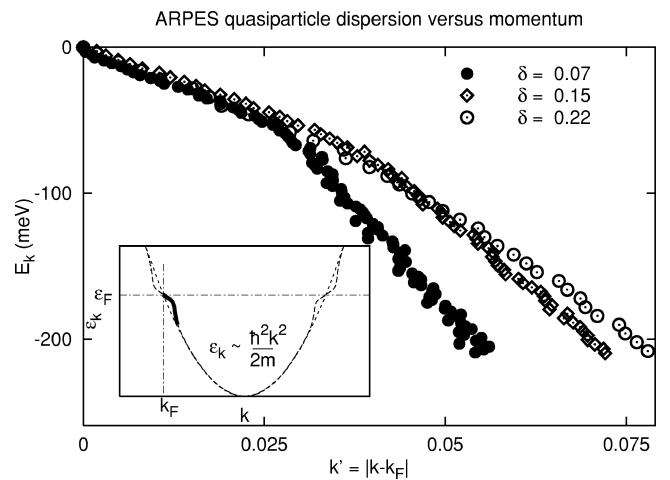

ARPES quasiparticle dispersion versus momentum

FIG. 1. Dispersion of occupied states vs momentum for LSCO with three different doping concentrations. The inset shows a schematic that puts this data in the context of a parabolic band. A modification due to electron-phonon coupling occurs near the Fermi surface. The region corresponding to the data of the main figure is highlighted in bold on the left side of the parabola.
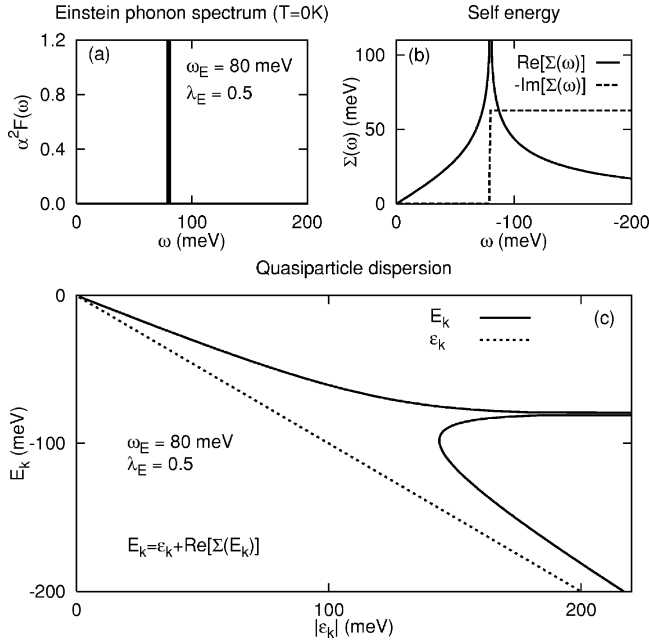
67 054503-1

FIG. 2. (a) Boson spectrum vs frequency, (b) The real and imaginary parts of the electron self-energy vs energy below the Fermi level, and (c) the resulting dispersion vs bare quasiparticle energy. These figures are for the Einstein model for phonons, with $\omega_E = 80$ meV and $\lambda_E = 0.5$. See text for a discussion of the multi-valued portion.

the temperature, thermal effects still do not reconcile theory with experiment. Example calculations are shown in Fig. 4. We use the full finite-temperature expression for the self-energy:[9]
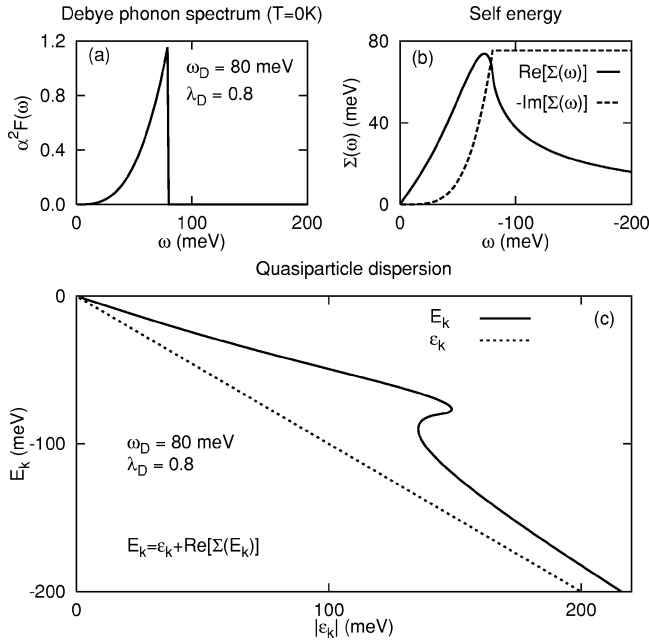

FIG. 3. Same as in Fig. 2, except for the Debye model, with $\omega_D = 80$ meV and $\lambda_D = 0.8$.
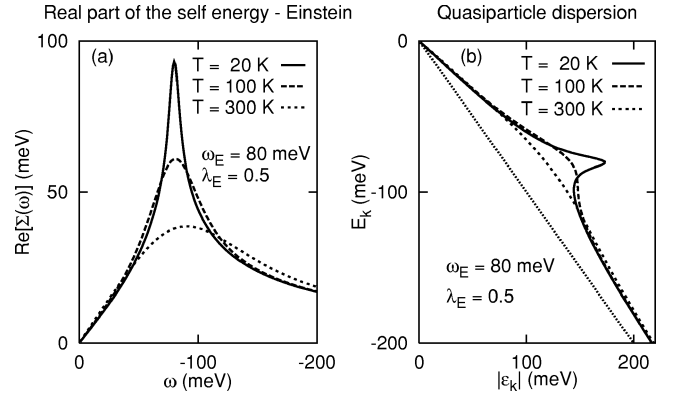

FIG. 4. Temperature dependence of (a) the real part of the self-energy, and (b) the dispersion relation for the Einstein model shown in Fig. 2. Note that the singularity is washed out by finite temperature.

$$\Sigma(\omega + i\delta) = \int_0^\infty d\nu\, \alpha^2 F(\nu) \left[-2\pi i (n(\nu) + 1/2) \right.$$

$$\left. + \psi\left(\frac{1}{2} + i\frac{\nu - \omega}{2\pi T}\right) - \psi\left(\frac{1}{2} - i\frac{\nu + \omega}{2\pi T}\right) \right], \quad (3)$$

where $\psi(x)$ is the digamma function and $n(\nu)$ is the Bose distribution function. Similarly, for the Debye model there is a well-pronounced shoulder, but still no clear kink. To determine what sort of spectrum leads to a kink, we utilize the procedure described below.

As a preliminary analysis, we note that the following function fits the data in the underdoped regime (where the kink is particularly prominent) reasonably well:

$$\Sigma_1(E_k) = \begin{cases} -\lambda E_k & \text{if } |E_k| < \omega_D \\ -\lambda \dfrac{\omega_D^2}{E_k} & \text{if } |E_k| > \omega_D . \end{cases} \quad (4)$$

This parametrization is motivated by the following considerations: we wanted an analytical form that would contain an explicit "kink," we wanted as simple a form as possible, and we wanted a form with which we could analytically perform the Kramers-Kronig integration to obtain the imaginary part of the self-energy. We have had to use an additional fit for the high-energy region to relate ϵ_k to $k - k_F$. For simplicity, we have used a linear fit, i.e., $\epsilon_k = xk'$, with $k' = |k - k_F|$. Inclusion of a quadratic term (see Ref. 10 for a discussion of quadratic corrections) results in a correction that is negligible. The proportionality constant x has units of eV Å and is related to the bare Fermi velocity ($x = \hbar v_F$). For the underdoped sample, the proportionality constant has been determined by the requirement that, at high energy, the full dispersion becomes the bare one (the model self-energy decreases to zero). Because the kink is washed out by increased doping, using the same function to fit the data in the optimally doped and especially in the overdoped regime is difficult. To overcome this problem we renormalize the momentum such that the three experimental curves overlap in the high-energy range. We then use the fit for the underdoped

Quasiparticle dispersion versus momentum
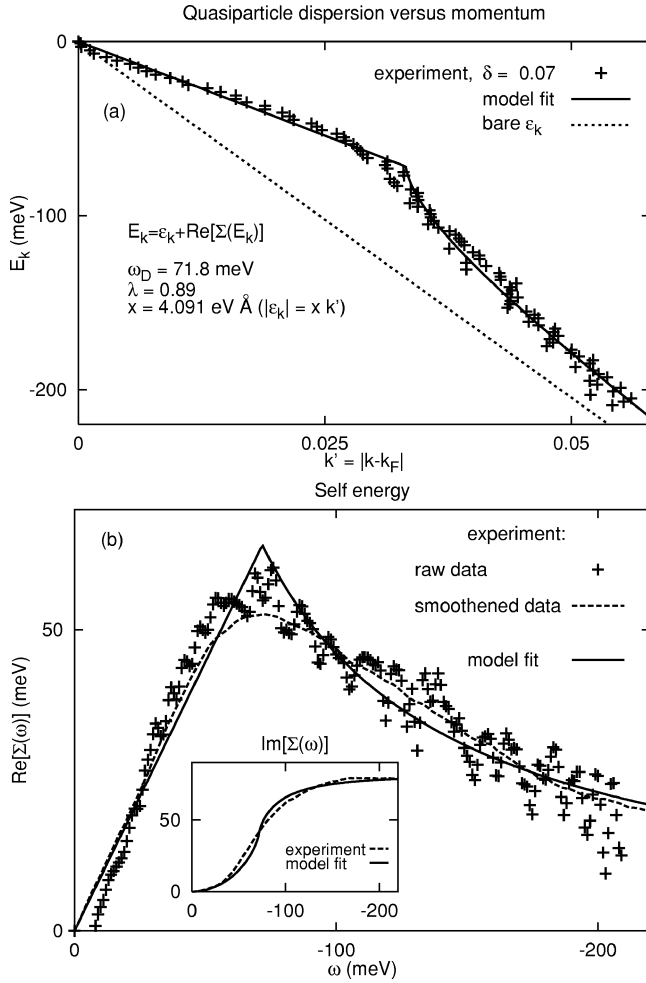
Self energy

FIG. 5. (a) The fit (solid curve) to the measured dispersion data (shown with symbols) for the underdoped case. We have used Eq. (3) with $\omega_D = 72$ meV and $\lambda = 0.89$. The dotted line shows the linear fit that results using $x = 4.1$ eV Å. (b) The real part of the self-energy vs energy, as extracted from the data (symbols), the model fit (solid curve), and the smoothened fit to the data (dashed curve). The inset shows the imaginary part obtained through Kramers-Kronig analysis.

data to calculate the proportionality constant x for the high-energy fit for the optimally doped and overdoped sample.

The result of using three fitting parameters λ, ω_D, and the background slope x is shown in Fig. 5; it is clear that the fit is very good. The important feature, captured by the fit, is the initial linear dependence of energy on wave vector, followed by an abrupt change at some characteristic frequency. In Fig. 5(b), we show the extracted real and imaginary parts of the self-energy from the data. We show the model fit, the actual data once the high-energy part is extracted, and the smoothened curve used to carry out the Kramers-Kronig analysis. We find parameter values of $\lambda = 0.89$, $\omega_D = 72$ meV, and $v_F = 4.1$ eV Å$/\hbar (= 6.2 \times 10^7$ cm/s). Varying these parameters, "by hand," results in a less than 10% change in λ, for example, before the fit becomes visually poor; we thus regard this as a rough measure of the uncertainty.
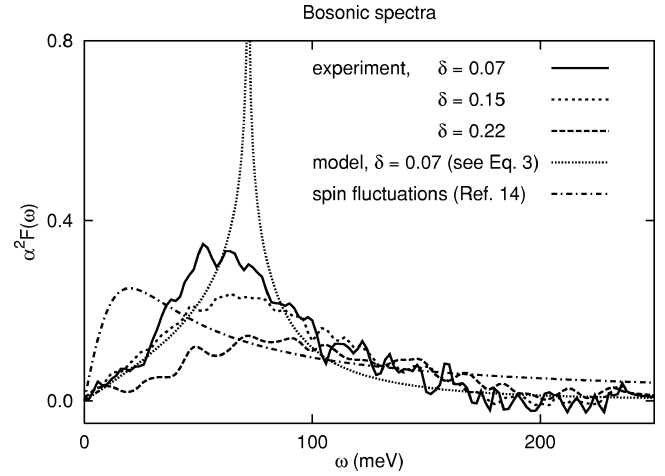
Bosonic spectra

FIG. 6. The bosonic spectral functions that result from an inversion of the data for underdoped, optimally doped, and overdoped samples (solid, short-dashed, and long-dashed curves, respectively). Parameters for the fits are given in Table. I. The model based on Eq. (3), designed specifically for the underdoped case, ($\delta = 0.07$), is also shown (dot-dashed curve) along with that expected for spin fluctuations (Ref. 14). In the spin fluctuation model of (Ref. 14) there is considerable spectral weight at high frequencies, including weight up to 400 meV (not shown). Note that in the inverted experimental results there are slight negative portions that are set to zero in the subsequent analysis in the text.

The imaginary part of the self-energy can be determined from the real part through a Kramers-Kronig integral

$$\Sigma_2(\omega + i\delta) - \Sigma_2(\infty + i\delta) = \frac{1}{\pi} \int_{-\infty}^{\infty} d\omega' \frac{\Sigma_1(\omega' + i\delta)}{\omega - \omega'}. \quad (5)$$

Substituting Eq. (4) results in

$$\Sigma_2(\omega + i\delta) - \Sigma_2(\infty + i\delta) = \frac{2}{\pi} \lambda \omega_D f(\omega/\omega_D), \quad (6)$$

where $f(x) = \frac{1}{2} + [(x^2 - 1)/4x] \ln|(1-x)/(1+x)|$. With the standard approximations,[9,11] one can relate the imaginary part of the self-energy to the underlying electron-phonon spectrum. The required result is

$$\alpha^2 F(\Omega) = -\frac{1}{\pi} \frac{d}{d\Omega} \Sigma_2(\Omega + i\delta). \quad (7)$$

The result from the fit shown in Fig. 5 is plotted in Fig. 6. Note that $f(x)$ is the same function that appears in the Hartree-Fock calculation for the free-electron gas,[12] and as is well known, its derivative has a logarithmic singularity at the characteristic frequency, as shown. Aside from the logarithmic singularity, the spectrum is peculiar (as an electron-phonon spectrum) in that it is linear at low frequencies, and has a long tail at high frequency. A model-independent calculation [i.e., without the fit given in Eq. (4)] for each of the doping concentrations, provided in Fig. 1, is also shown in Fig. 6. There is clearly a rounding of the singularity,[13] although the overall strength of the interaction, as indicated by the area under the spectrum, is of the same magnitude.

TABLE I. Spectral function parameters as a function of dopant concentration. The parameters λ and $\omega_{\ln}$ are determined by numerical integrals (Ref. 9) for the spectral functions shown in Fig. 6. All indicators show a somewhat enhanced coupling at optimal doping.

Dopant level	$\delta=0.07$	$\delta=0.15$	$\delta=0.22$
λ	0.94	0.82	0.51
$\omega_{\ln}$ (meV)	42	40	38
T_c (K)	58	46	19

Several questions arise from the results of Fig. 6. First, what sort of coupling strength do these spectra represent, as measured by a superconducting critical temperature, assuming that these are utilized in an Eliashberg-type analysis? To answer this question, one would ideally like to perform a calculation with an order parameter with d wave symmetry. However, for this to be meaningful one would require a series of results as shown in Fig. 1 for various directions in the Brillouin zone. Then the same inversion scheme would result in a momentum-dependent spectrum, which would then be used in a d-wave Eliashberg equation. Since this information is lacking, we simply use an s-wave calculation, with the direct Coulomb interaction set to zero. This would apply if the repulsion was primarily short ranged; then the d-wave symmetry would be unaffected by it. On the other hand, there is no guarantee that the momentum dependence of the data acquired in this way would necessarily lead to d-wave superconductivity. We proceed in this simplistic way nonetheless, and obtain the results for the three doping concentrations summarized in Table I. As judged both by the value of T_c and the parameter λ, the coupling strength decreases as the doping increases. Probably the data from more dopant concentrations are required before one can assess how significant this trend is, and what additional physics may cause T_c to decrease in the underdoped regime. We should emphasize that the main part of the analysis is done in the normal state. Since momentum-dependent data is lacking, we have tacitly assumed that the coupling strength is independent of momentum; an important refinement will be to eventually try to extract this momentum dependence and see how it correlates with d-wave pairing.

Another interesting question is whether these spectral functions represent phonons or not. As pointed out in Ref. 7, the most compelling evidence favoring phonons is that the frequency domain is consistent with that observed in neutron scattering. Figure 6 does show high-frequency spectral weight, however, and one can ask whether these high-frequency tails (clearly beyond the phonon energies in these materials) rule out phonons as a possibility. To address this question we cut off the spectrum at 100 meV, and then readjusted other parameters in the fit (by hand) to recover an improved fit to the data originally presented in Fig. 1. While the fit is never as good as the original one, we find that it is sufficiently good to be a plausible possibility. Thus, unfortunately, we are unable to say anything very definite on this issue. It is true that spin fluctuations (one of the competing alternatives to phonons) are expected to have significant spectral weight at higher frequency. An example is shown in
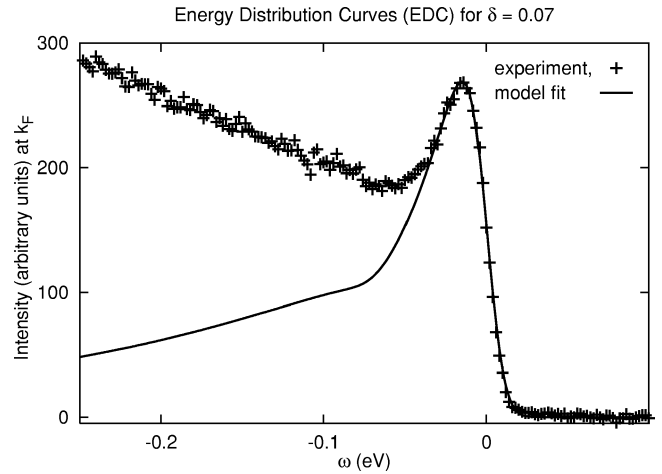

FIG. 7. The energy distribution function [spectral function times the fermi function convoluted with an energy-resolution function (Ref. 15)] vs energy, for the underdoped sample, at k_F. The impurity scattering rate used was $1/\tau=80$ meV, and the energy broadening was 8 meV. The fit is excellent at low energy, but clearly fails at high energy.

Fig. 6, taken from Ref. 14, which has considerable spectral weight extending up to 400 meV. It is clear that significant spectral weight exists at frequencies much higher than indicated by the experimental data. Furthermore, this particular spectrum appears to be considerably softer below the 50-meV region than the data indicates. Once again more definite statements could be possible once a detailed momentum dependence of the spectral functions is available.

Finally, we have focused on the real part of the dispersion. One might as well ask why we did not examine the imaginary part directly. The partial answer to this question is that there are other (i.e., nonpairing) scattering processes that affect the imaginary part of the self-energy and not the real part (e.g., impurities — see below). Even more critically, as was attempted in the original angle-resolved photoemission spectroscopy (ARPES) inversion work,[6] one might try to invert the entire spectral function. The difficulty is exemplified in Fig. 7, where we show an energy distribution curve taken at k_F for the underdoped sample. We have also plotted the energy distribution calculated with our model fit for the self-energy, Eqs. (4) and (6), additionally including an energy-resolution function[15] and elastic scattering from impurities (which affects the imaginary part of the self-energy, but not the real part). The fit is excellent at low energies, but there is a clear and very large discrepancy at high energies. The origin of this discrepancy is simply not understood at present. It may or may not represent new physics (there may be a lack of understanding in the analysis of ARPES), but it clearly will not be understood with the approach adopted in this paper, which focuses on the quasiparticle peak as an essential feature. Mainly for this reason we felt that an examination of the real part of the self-energy (i.e., the dispersion) was the best procedure for extracting a potential pairing interaction.

In summary, we have used the electron dispersion, as measured by ARPES, to extract an electronic self-energy (real part). Through Kramers-Kronig we are able to extract

the imaginary part of the self-energy, from which an inelastic scattering spectral function is extracted in a straightforward manner. The result is summarized in Fig. 6 for a variety of doping concentrations in LSCO. The result is clearly compatible with phonons; the extracted coupling strength would then be able to account for the superconductivity. However, based on the available data we are unable to rule out, for example, spin fluctuations as a possibility. Measurements over more doping concentrations and in different directions in the Brillouin zone would aid considerably in narrowing down the possibilities.

[1] J.M. Rowell, P.W. Anderson, and D.E. Thomas, Phys. Rev. Lett. **10**, 334 (1963).

[2] W.L. McMillan and J.M. Rowell, Phys. Rev. Lett. **14**, 108 (1965).

[3] N. Tsuda, K. Nasu, A. Fujimori, and K. Siratori, *Electronic Conduction in Oxides*, 2nd ed. (Springer, New York, 2000), and references therein.

[4] F. Marsiglio, T. Startseva, and J.P. Carbotte, Phys. Lett. A **245**, 172 (1998); F. Marsiglio, Mol. Phys. Rep. **24**, 73 (1999).

[5] J.P. Carbotte, E. Schachinger, and D.N. Basov, Nature (London) **401**, 354 (1999).

[6] G.B. Arnold, F.M. Mueller, and J.C. Swihart, Phys. Rev. Lett. **67**, 2569 (1991); J.C. Swihart, W.H. Butler, F.M. Mueller, and G.B. Arnold, Phys. Rev. B **46**, 5861 (1992).

[7] A. Lanzara, P.V. Bogdanov, X.J. Zhou, S.A. Kellar, D.L. Feng, E.D. Lu, T. Yoshida, H. Eisaki, A. Fujimori, K. Kishio, J.-I. Shimoyama, T. Noda, S. Uchida, Z. Hussain, and Z.-X. Shen, Nature (London) **412**, 510 (2001).

[8] S. Englesberg and J.R. Schrieffer, Phys. Rev. **131**, 993 (1963).

[9] P.B. Allen and B. Mitrović, in *Solid State Physics*, edited by H. Ehrenreich, F. Seitz, and D. Turnbull (Academic, New York, 1982), Vol. 37, p. 1.

[10] S. LaShell, E. Jensen, and T. Balasubramanian, Phys. Rev. B **61**, 2371 (2000).

[11] F. Marsiglio and J.P. Carbotte, in *The Physics of Conventional and Unconventional Superconductors*, edited by K.H. Bennemann and J.B. Ketterson (Springer-Verlag, Berlin, 2003) p. 233; F. Marsiglio and J.P. Carbotte, cond-mat/0106143 (unpublished).

[12] N.W. Ashcroft and N.D. Mermin, *Solid State Physics* (Saunders, New York 1976), p. 334.

[13] This is due to two reasons: first, the data does not, after all, display a perfect kink, and second, we have had to employ some smoothing to the data to perform the Kramers-Kronig and subsequent analyses.

[14] E. Schachinger, J.P. Carbotte, and D.N. Basov, Europhys. Lett. **54**, 380 (2001).

[15] R. Fehrenbacher, Phys. Rev. B **54**, 6632 (1996).